Applied Surface Science 607 (2023) 154875

Contents lists available at ScienceDirect

Applied Surface Science

journal homepage: www.elsevier.com/locate/apsusc

Full length article

Self-organized formation of unidirectional and quasi-one-dimensional metallic Tb silicide nanowires on Si(110)

Stephan Appelfeller [a,b,*], Martin Franz [a], Murat Karadag [a], Milan Kubicki [a], Robert Zielinski [a,c], Maxim Krivenkov [d], Andrei Varykhalov [d], Alexei Preobrajenski [b], Mario Dähne [a]

[a] Institut für Festkörperphysik, Technische Universität Berlin, D-10623 Berlin, Germany
[b] MAX IV Laboratory, Lund University, SE-221 00, Lund, Sweden
[c] Leibniz-Institut für Analytische Wissenschaften – ISAS – e.V., D-12489 Berlin, Germany
[d] Helmholtz-Zentrum Berlin für Materialien und Energie, D-12489 Berlin, Germany

ARTICLE INFO

Keywords:
Nanowires
Silicides
LEED
STM
STS
PES
ARPES
Growth
Electronic structure

ABSTRACT

Terbium induced nanostructures on Si(110) and their growth are thoroughly characterized by low energy electron diffraction, scanning tunneling microscopy and spectroscopy, core-level and valence band photoelectron spectroscopy, and angle-resolved photoelectron spectroscopy. For low Tb coverage, a wetting layer forms with its surface fraction continuously decreasing with increasing Tb coverage in favor of the formation of unidirectional Tb silicide nanowires. These nanowires show high aspect ratios for high annealing temperatures or on substrates already containing Tb in the bulk. Both wetting layer and nanowires are stable for temperatures up to 750 °C. In contrast to the nanowires, the wetting layer is characterized by a band gap. Thus, the metallic nanowires, which show a quasi-one-dimensional electronic band structure, are embedded in a semiconducting surrounding of wetting layer and substrate, insulating the nanowires from each other.

1. Introduction

Covering clean Si substrates with thin layers of Tb and annealing may lead to the self-organized growth of nanosized surface structures that consist of Tb disilicide, a compound that also exists as a bulk material [1–4]. Thus such nanostructures combine two enticing aspects: Firstly, if their dimensions are small enough, they represent low-dimensional systems, i.e., they are expected to show quantum confinement effects [5] and other exotic two-dimensional or one-dimensional electronic properties [6,7]. Secondly in contrast to most adsorbate-induced surface structures, they have an application perspective, since Tb silicides can be embedded in a Si matrix while preserving their structure [8–10].

On Si(111), there is a very good lattice match of the unreconstructed surface with the *c*-plane of the hexagonal Tb disilicide. A similar structural match, however with a small anisotropic lattice mismatch, exists between Si(001) and the *m*-plane of the hexagonal Tb disilicide. This enables the epitaxial growth of the Tb disilicide on these substrates leading to two-dimensional layers on Si(111) [11,12] and to nanowires on Si(001) [3]. In contrast, there is no low index Tb disilicide plane fitting well with the Si(110) surface. Nevertheless, there are reports on the growth of nanowires on Si(110) for other trivalent rare-earth metals [13–15]. Due to the strong chemical similarity of all trivalent rare-earth metals, a similar nanowire formation is expected for Tb on Si(110).

In this article, we study the formation of Tb induced nanostructures on Si(110) and their properties using a wide range of experimental techniques: low energy electron diffraction (LEED), scanning tunneling microscopy (STM) and spectroscopy (STS), core-level and valence band photoelectron spectroscopy (PES), and angle-resolved photoelectron spectroscopy (ARPES). Indeed, the formation of unidirectional Tb silicide nanowires is found with a wetting layer in between, the latter covering the entire surface for low Tb coverage. The nanowires show huge aspect ratios, especially for high annealing temperatures or substrates already containing Tb. A finite density of states at the Fermi level is found for the nanowires by valence band PES and STS. In contrast, the surrounding wetting layer is characterized by a band gap at the Fermi level. Finally, we observe a quasi-one-dimensional band in ARPES that is assigned to the nanowires.

2. Experimental details

Measurements were carried out at four different ultra-high vacuum chamber systems, each consisting of separate preparation and

* Corresponding author at: MAX IV Laboratory, Lund University, SE-221 00, Lund, Sweden.
E-mail address: stephan.appelfeller@physik.tu-berlin.de (S. Appelfeller).

https://doi.org/10.1016/j.apsusc.2022.154875
Received 17 June 2022; Received in revised form 29 August 2022; Accepted 9 September 2022
Available online 20 September 2022

measurement chambers. All systems are equipped with LEED optics to determine the grown surface structures, in this way allowing a consistent characterization of the same structures at the different experimental setups. In addition to LEED, sample cross referencing was also done using PES data for the two PES stations. All measurements were performed at room temperature.

The sample preparation followed the same recipe for all systems. Samples were cut from commercial *n*-type Si(110) wafers. They were cleaned *ex-situ* by rinsing with water and ethanol and *in-situ* by degassing at 600 °C followed by repeated flash annealing up to 1150 °C. The samples were heated by direct current and their temperature was measured using infrared pyrometers (ΔT = 20 °C and emissivity setting ϵ = 0.67 for all temperatures). For the preparation of well-ordered clean Si(110) surfaces, the samples were slowly cooled down to room temperature from about 800 °C. The nanostructures were grown by deposition of Tb on the clean Si(110) substrates and annealing during or after the metal deposition (post deposition annealing duration $\leq$ 2 min). Terbium was evaporated from home-built electron-beam evaporators using W crucibles and the deposited amount was determined by the deposition rate and time. The deposition rates were measured by quartz crystal microbalances (accuracy ±20%) and cross-checked with the known phase diagram of Tb induced structures on Si(111) [11]. It should be noted that the definition of one monolayer (ML) on Si(110) is not consistent throughout the literature. In this work, 1 ML corresponds to the density of surface atoms on the unreconstructed Si(110) surface of 9.59 × 10^{14} atoms/cm^2, i.e., 2 atoms per 1 × 1 unit cell.

STM and STS measurements were carried out at the Technische Universität Berlin using a home-built STM with a Nanonis (SPECS) control unit. For the verification of the substrate cleanliness at the MAX IV Laboratory, further STM measurements were done using a VT XA STM by Scienta-Omicron at the Surface Probe Microscopy Lab. The microscopes hosted electrochemically etched W tips, which were cleaned *in-situ* by electron bombardment. All images were taken in constant current mode with a tunneling current of I_T = 100 pA and the sample voltages V_S given at the images. STS spectra were obtained as point spectra with and without vertical tip displacement after the feedback loop was switched off. The STM images were analyzed using the WSXM and Gwyddion software [16,17].

High-resolution PES measurements of core-levels and valence bands were performed in normal emission geometry at the Surface and Material Science branch end station of the FlexPES beamline at the MAX IV Laboratory, which was equipped with a Scienta SES-2002 photoelectron analyzer. ARPES and additional PES data were obtained at the 1^2 ARPES ultra high resolution photoemission station at the UE112 PGM-2a-1^2 beamline of BESSY II (Helmholtz Zentrum Berlin), which hosts a Scienta R8000 photoelectron analyzer.

3. Results and discussion

3.1. Formation of Tb induced nanostructures

3.1.1. Overview on the surface structures

The contamination free Si(110) surface is characterized by a two-domain reconstruction given by the matrices

$$\begin{pmatrix} 1 & 17 \\ 2 & 2 \end{pmatrix} \text{ and } \begin{pmatrix} 1 & -17 \\ 2 & -2 \end{pmatrix}.$$

This reconstruction will be referred to as 16 × 2 structure in this work, as it is typical in the literature [18–21]. A LEED pattern of this reconstruction is shown in Fig. 1(a) and a corresponding STM image is depicted in Fig. 2(a). In real space, the 16 × 2 reconstruction is characterized by corrugated stripes in the $\langle 1\bar{1}2 \rangle$ directions, which form with two distinct heights separated by single steps (step height of 0.19 nm). The distance between stripes of the same height amounts to 5.02 nm leading to the densely spotted lines in the $\langle 1\bar{1}1 \rangle$ directions in LEED patterns. In general, two domains of the 16 × 2 reconstruction

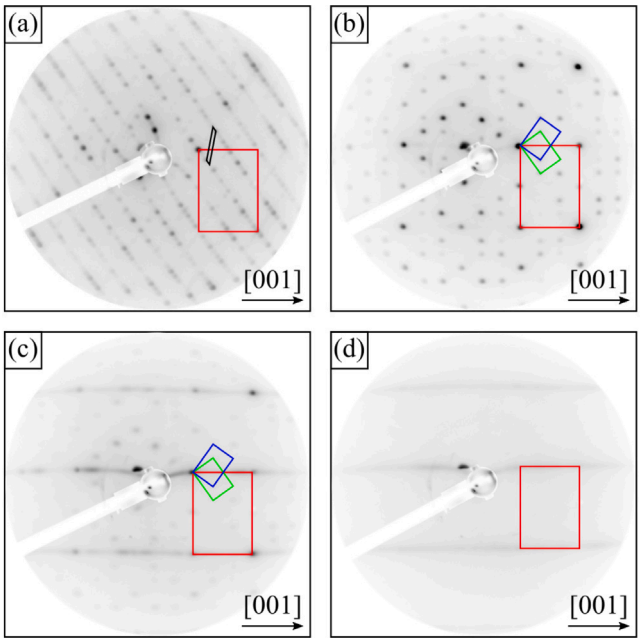

Fig. 1. LEED patterns of (a) a clean Si(110) surface, (b) a surface dominated by the wetting layer, (c) a mixture of wetting layer and nanowires on the Si(110) surface, and (d) a dominant nanowire formation (E_{kin} = 66 eV for all images). The red rectangles mark 1 × 1 reciprocal unit cells, the black parallelogram in (a) one of the 16 × 2 reconstruction, and the blue and green rectangles in (b) and (c) the ones of the wetting layer.

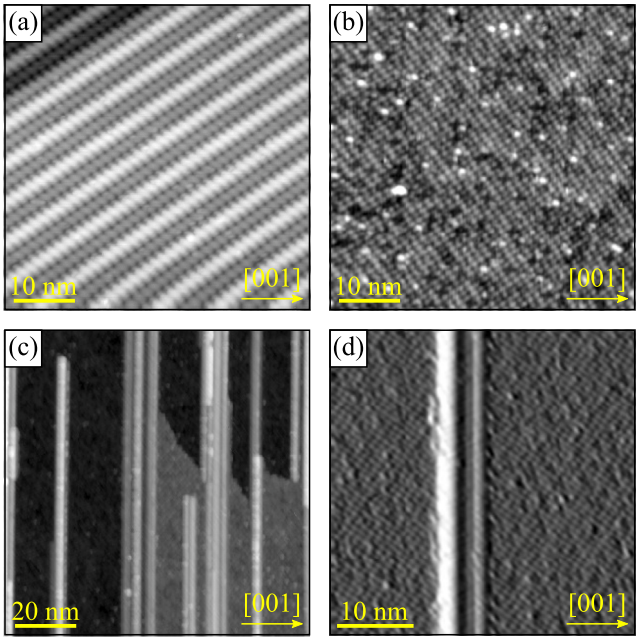

Fig. 2. STM images of (a) a pristine Si(110) substrate (V_S = +1.5 V), (b) a Si(110) surface covered by the Tb induced wetting layer (V_S = −2.5 V), and (c) a nanowire preparation (V_S = −1.5 V). In (d), the topographic STM image is merged with its derivative to highlight the corrugation of the wetting layer in between the nanowires (V_S = −2.0 V).

are observed, but the dominant formation of a single domain is also possible [20,21], as seen in the shown LEED pattern [Fig. 1(a)].

Depositing a submonolayer amount of Tb and annealing at temperatures around 500 °C changes the surface morphology drastically, as a Tb induced wetting layer forms. According to LEED and STM

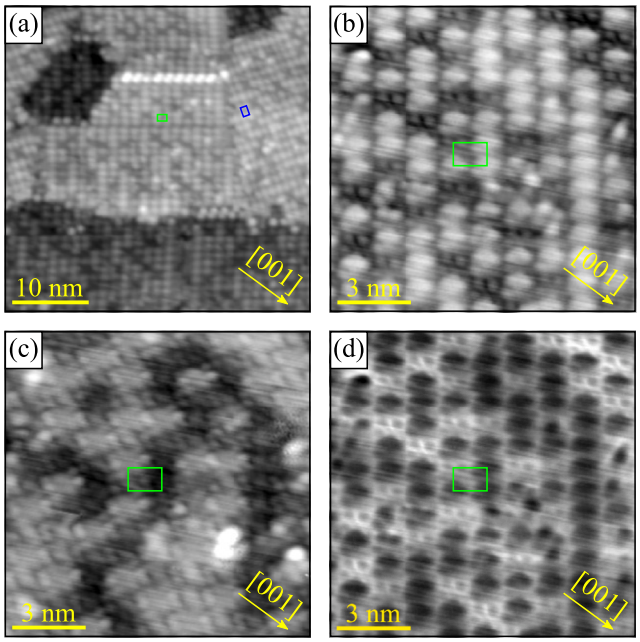

Fig. 3. (a) STM image of a wetting layer preparation on a pristine substrate (V_S = −2.5 V). The green and blue rectangles mark the differently oriented unit cells of the two domains. (b, c) Simultaneously acquired detailed STM images of (b) filled states (V_S = −1.5 V) and (c) empty states (V_S = +1.5 V). (d) Contrast inverted STM image of (b).

data, the wetting layer is characterized by rows in the $\langle 1\bar{1}1\rangle$ directions [Figs. 1(b) and 2(b)]. In contrast to the 16 × 2 reconstruction of the clean substrate, the LEED patterns of the wetting layer obtained here always show two domains.

Increasing the amount of deposited Tb leads to the formation of Tb silicide nanowires. In contrast to the stripes of the clean substrate and the wetting layer, the nanowires grow along the $[1\bar{1}0]$ direction [Fig. 2(c)]. Due to the symmetry of the substrate, the nanowires form in a single domain, thus being parallel across the entire substrate surface. In LEED, the nanowire formation leads to streaks in the [001] direction, i.e., perpendicular to the nanowires, while they are characterized by a ×1 periodicity in $[1\bar{1}0]$ direction, i.e., along the nanowires [Fig. 1(c) and (d)]. Typically, the wetting layer is present between the nanowires [Figs. 1(c) and 2(d)], but for very high Tb coverage the surface is largely dominated by the nanowires [Fig. 1(d)].

In the following, the growth of the Tb induced nanostructures and their structural characteristics as observed by STM will be discussed in more detail.

3.1.2. The Tb induced wetting layer

Fig. 3(a) shows an STM image of a preparation using a fresh Si(110) substrate, a Tb coverage of 0.1 ML, and annealing to 500 °C during the metal deposition. The entire surface is covered by the Tb induced wetting layer and neither the stripes of the 16 × 2 reconstruction of the clean substrate nor any nanowires were observed on this sample. Thus such a low Tb coverage is sufficient to lead to a complete restructuring of the surface, but insufficient to enable the formation of Tb silicide nanowires on pristine Si(110) substrates at least for such low annealing temperatures.

In filled states images, e.g., Fig. 3(a), the wetting layer is characterized by oval protrusions that are separated by (1.4 ± 0.2) nm in the $\langle 1\bar{1}2\rangle$ directions and (0.9 ± 0.1) nm in the $\langle 1\bar{1}1\rangle$ directions. These values agree very well with the periodicity observed in LEED [Fig. 1(b)]. The superstructures corresponding to the two domains of the wetting layer are the $(\sqrt{6}\times\sqrt{6})$R35.3° reconstruction and the equivalent, but mirror-symmetric $(\sqrt{3}\times 2\sqrt{3})$R54.7° reconstruction, which were also observed for Y on Si(110) [15].

The wetting layer shown in Fig. 3(a) is characterized by rather small domains due to the low annealing temperature employed during this preparation. This low annealing temperature is also the reason for the observation of the monolayer-high steps leading to holes in the terraces. Higher annealing temperatures lead to larger wetting layer domains without any holes, often covering entire terrace segments defined by steps or nanowires, such as the preparation shown in Fig. 2(b), where an annealing temperature of 750 °C was used. However, for all preparations studied by STM, i.e., for annealing temperatures between 400 °C and 750 °C and for Tb coverages between 0.1 ML and 1.9 ML, the wetting layer always showed a rather high defect density.

Filled and empty states STM images of the very same area are shown in Fig. 3(b) and (c), respectively. The filled states image is again dominated by oval protrusions. In contrast, the protrusions observed in the empty states image are less well defined, and the unit cell is not easily recognizable. Comparing both images, bright appearing structures in the filled states image can be assigned to dark appearing structures in the empty states image and *vice versa*. This is especially evident when comparing the contrast inverted filled states image of Fig. 3(b), shown in Fig. 3(d), with the empty states image [Fig. 3(c)]. Although not explicitly stated in Ref. [15], the same polarity dependent contrast inversion is also observed for Y as rare earth metal, see Fig. 2(a) and (b) of Ref. [15].

The currently available data are not sufficient for the proposal of a convincing structure model for the wetting layer. However, the structural units of the wetting layer are certainly different from the building blocks known from the clean substrate [compare Fig. 2(a) and (b)]. Thus, one can exclude a Tb induced rearrangement of these building blocks, which is, e.g., observed for a low concentration Ni contamination on Si(110) [19,22,23]. Assuming the presence of Tb atoms within the structural units of the wetting layer, the 0.1 ML Tb deposited during the preparation shown in Fig. 3(a) correspond to an average of 1.2 Tb atoms per unit cell. Now there are at least two plausible scenarios in agreement with the observed surface morphology. Firstly, all unit cells of the wetting layer could contain either one or two Tb atoms each, leading to two states of the structural units with bright or dark appearance in the images. Secondly, the different appearing structural units could be caused by the presence or absence of a Tb atom pair per unit cell. Thus, for the development of a structure model, more data for low Tb coverage on pristine substrates, possibly revealing a coverage dependent ratio of the frequency of the two structural units, and theoretical calculations would be beneficial, but beyond the scope of the present study.

The wetting layer depicted in Fig. 3(b) and (c) was prepared by flash annealing a sample with a previous Tb silicide nanowire preparation and slowly cooling down to room temperature afterwards, but without any additional deposition of Tb. Thus, similar to observations for other Si substrates, Tb segregates into the Si bulk during flash annealing and diffuses back to the surface upon cooling down [2,4,24]. On the one hand, this prevents the recovery of the 16 × 2 reconstruction of the clean substrate by flash annealing. On the other hand, it was not possible to grow nanowires only by flash annealing and cooling down without any further Tb deposition even if large amounts of Tb have been deposited on this Si(110) substrate beforehand. However, previous preparations influence the nanowire growth as will also be elucidated in the following.

3.1.3. The Tb silicide nanowires

Fig. 4(a) and (b) show nanowire preparations using pristine Si(110) substrates, a Tb coverage of 0.35 ML, and annealing at 500 °C for 2 min after or during the metal deposition, respectively. While the nanowires are slightly longer and agglomerated in wider nanowire bundles for annealing during the Tb deposition, the general growth behavior is

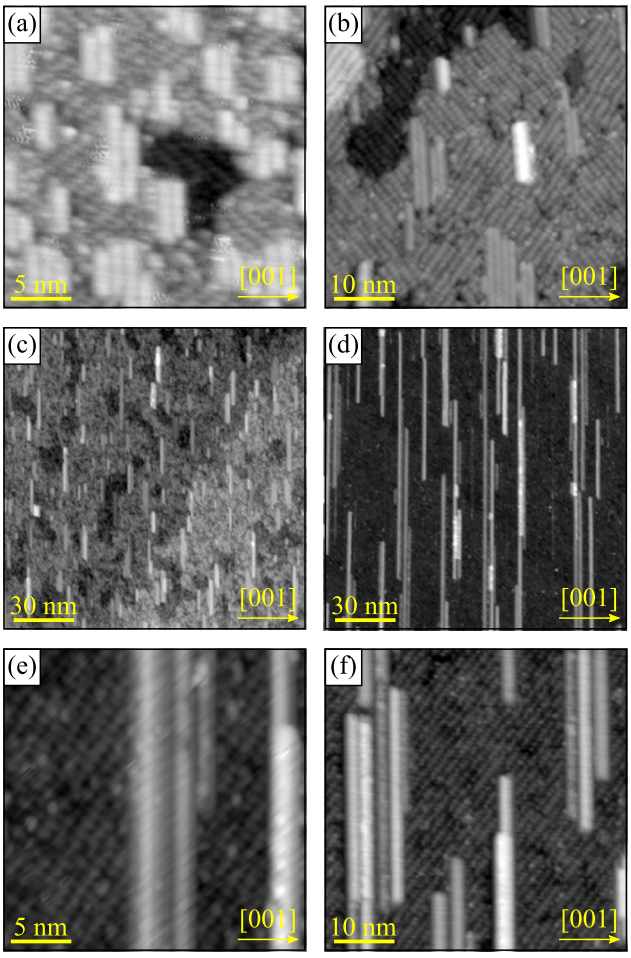

Fig. 4. STM images of nanowire preparations using an annealing temperature of 500 °C. (a–c) Preparations on pristine substrates [(a) $V_S = -1.5$ V, (b) $V_S = -2.5$ V, and (c) $V_S = -1.5$ V]. (d–f) Preparations on reused substrates [(d) $V_S = -2.5$ V, (e) $V_S = -1.5$ V, and (f) $V_S = -1.5$ V]. The apparent corrugation along the nanowires in (e) is probably related to a vibration.

similar for both preparations. Although most of these nanowires are very narrow with widths below 2 nm, their aspect ratios are rather small. The wetting layer between the nanowires is characterized by small domains and terraces with monolayer-deep holes, as already observed for the wetting layer preparation at the same low annealing temperature of 500 °C [Fig. 3(a)]. This porousness of the terraces is particularly well seen in the overview image of the preparation using annealing during the Tb deposition, which is shown in Fig. 4(c).

The nanowire growth drastically changes when a substrate is used that was cleaned by flash annealing after a prior Tb deposition. Cleaning and applying the same nanowire preparation procedure a second time to the sample shown in Fig. 4(b) and (c) leads to the surface depicted in Fig. 4(d) and (e). Now the nanowires extend much longer leading to much higher aspect ratios even though the median full width at the nanowire base is increased to (3.4 ± 0.3) nm. In addition, the wetting layer formation is more uniform and there are no holes any more in its terraces. As an additional example, a similar change in growth behavior is observed for the sample shown in Fig. 4(a). After cleaning by flash annealing and depositing 0.35 ML Tb at 500 °C, nanowires with increased aspect ratios and a uniform wetting layer are found [Fig. 4(f)].

However, it is not necessary to use a substrate multiple times to achieve the growth of nanowires with high aspect ratios. A higher annealing temperature of 600 °C during the Tb deposition is also sufficient even when a pristine Si(110) substrate is used [Fig. 5(a)]. Nevertheless, an increase of the average length of the formed nanowires is also observed for an annealing temperature of 600 °C when a substrate is reused [Fig. 5(b)].

Further increasing the annealing temperature to 750 °C leads to even more extreme aspect ratios [Fig. 5(c)]. The nanowire lengths exceed 500 nm (limited by the areas studied), while the median full width at the nanowire base is about 7 nm. For this preparation, we observed very rarely nanowire endings and no nanowire along its whole length within the analyzed area, so that the termination of the nanowires directly outside of the studied area is unlikely. Thus, we may assume lengths in the μm range and therewith nanowire aspect ratios (much) larger than 100. Terbium silicide nanowires with such huge aspect ratios are typically only observed on vicinal Si substrates [3,4,10], but here they are possible using planar substrates due to the unidirectional growth of the nanowires.

In contrast to the length to width ratio, the width to height ratio was below 10 for all analyzed nanowires, since the average height increases with the nanowire width, although large variations in the apparent heights are found for each nanowire width. However in the exemplary tip-height profile in Fig. 5(e), both nanowires show widths of about 7.3 nm and apparent heights of about 1.3 nm. In this profile, the nanowires are characterized by triangular shapes, which show two differently inclined flanks in each case. Such a shape is found even for wide nanowires and high resolution images, which is in contrast to the findings for Tb silicide nanowires on planar Si(001), for which plateaus parallel to the substrate surface may be observed at their top [3]. Consequently, the nanowire structure on Si(110) may be characterized by a triangular cross section.

In general, the observation of nanowires for an annealing temperature of 750 °C is remarkable, since it is in contrast to the growth of Tb silicide structures on Si(001) [3]. On Si(001) substrates, the growth of nanowires is only observed within a certain annealing temperature window, while high annealing temperatures of 700 °C lead to the formation of compact and rather high Tb silicide islands as the energetically most favorable Tb induced surface structures. This difference between the Si substrates is presumably related to the existence and the missing of bulk Tb silicide planes laterally matched to the Si(001) and Si(110) surfaces, respectively. Furthermore on Si(001), high annealing temperatures also lead to the observation of the clean substrate in between Tb silicide structures, while the Tb induced wetting layer is still present between the nanowires on Si(110) substrates [Fig. 5(d)].

For the preparation shown in Fig. 5(c) and (d), 1.9 ML Tb were deposited. Thus, the rare earth metal coverages and the annealing temperatures are similar to the ones used for the growth of Ce, Er, and Gd silicide nanowires on Si(110) [14,25,26]. However, there are large differences between these reported nanowire structures and the ones found here, which are presumably related to the rather short annealing periods after the metal deposition in the present study. In contrast, our observations are in agreement with a report on Dy silicide nanowires on Si(110) [13], in which also similar preparation parameters were used.

In Ref. [13], a structural and a growth model were proposed for the Dy disilicide nanowires based on transmission electron microscopy data. It was found that the nanowires form on {111} facets and grow endotaxially, i.e., partially into the substrate, and the nanowire formation was explained by kinetic effects, i.e., a faster silicide growth along the surface than into the surface. A further energetic reason for the nanowire formation may be the easier strain relaxation in elongated islands [27]. Due to the strong similarities between the trivalent rare earth disilicides, we assume that a related structure and growth model may be adopted for the present Tb silicide nanowires, also considering that a disilicide growth on the Si(111) surface is energetically favorable because of the negligible lattice mismatch [2,12].

In this growth model, the nanowires grow in a single domain showing that the rare earth disilicides form either on (111) or on $(11\bar{1})$ facets, which share the $[1\bar{1}0]$ nanowire growth direction with the Si(110)

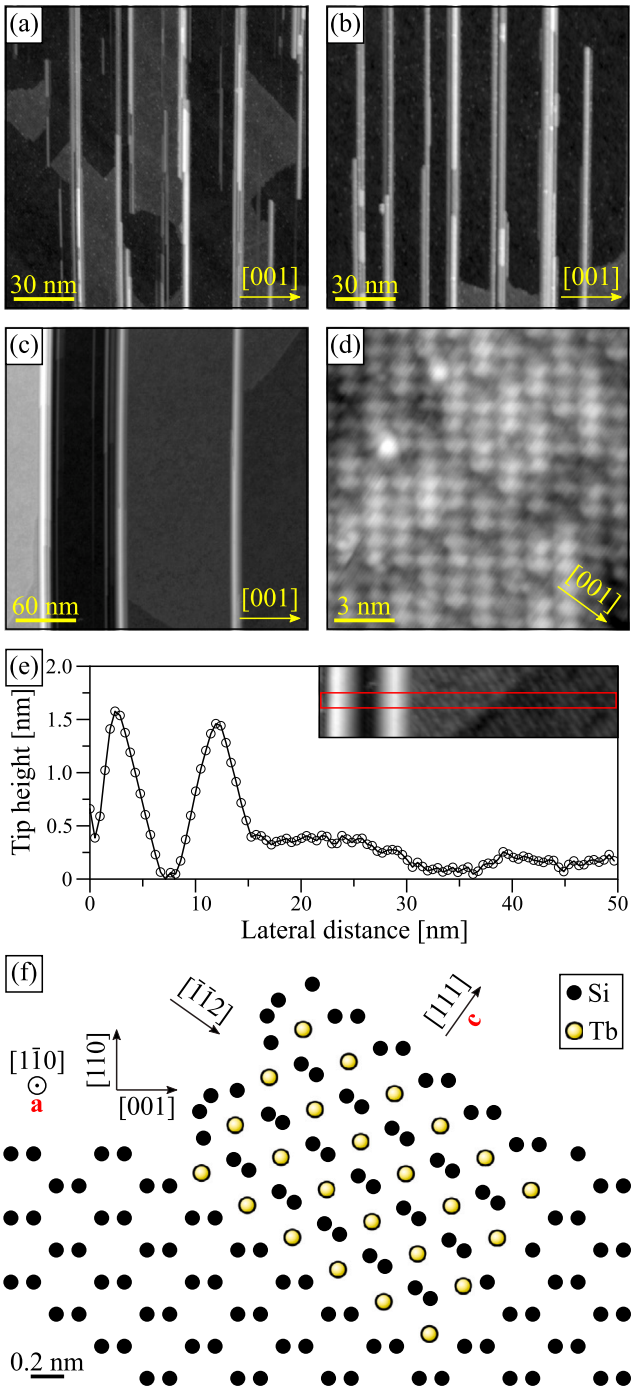

Fig. 5. (a, b) STM images of nanowire preparations with annealing at 600 °C during the deposition of 0.4 ML Tb using (a) a pristine substrate and (b) the same substrate after cleaning by flash annealing between the two preparations [(a) V_S = −2.5 V and (b) V_S = −1.5 V]. (c) Overview STM image of a preparation with an annealing temperature of 750 °C (V_S = −1.5 V). (d) Detailed STM image of the surface in between the nanowires for the preparation shown in (c) (V_S = −1.5 V). (e) Height profile over two nanowires observed for the preparation shown in (c) along the red box marked in the inset. (f) Proposed structure model of the nanowires with the *c*- and *a*-axes of the hexagonal Tb disilicide parallel to the [111] and [1$\bar{1}$0] directions of the substrate, respectively.

surface and have inclination angles of about 35° with respect to the substrate plane. In contrast, no nanowire formation is observed on {1$\bar{1}$1} and {1$\bar{1}\bar{1}$} facets, which would result in nanowires parallel to the [1$\bar{1}\bar{2}$] and [1$\bar{1}$2] directions, respectively. However, the {1$\bar{1}$1} and {1$\bar{1}\bar{1}$} facets are perpendicular to the substrate and, consequently, rare earth disilicide formation on them would require an additional energetically unfavorable bottom interface. Thus the preferential silicide formation occurs with (111) and (11$\bar{1}$) facets.

A possible nanowire cross section based on this structure model is depicted in Fig. 5(f). The nanowire with its hexagonal structure grows along its *a*-axis. The *c*-axis of the Tb disilicide, along which Tb and Si planes alternate, is inclined with respect to the surface normal leading to a triangular cross section within and presumably also outside of the Si(110) substrate. This is in agreement with the finding of triangular shapes with two different inclination angles in tip-height profiles over the nanowires such as in Fig. 5(e). In the structure model, the substrate-nanowire interface on the (111) facet is well-determined [left in Fig. 5(f)], while it is uncertain if certain facets may dominantly form at the second interface [right in Fig. 5(f)].

In contrast to the endotaxial growth mode observed in Ref. [13], a different structure was proposed for Y silicide nanowires on Si(110) based solely on STM data, assuming a purely epitaxial growth of the nanowires [15]. Although such a structure seems improbable on the first view when taking into account the electron microscopy data [13], the low temperature nanowire growth on pristine substrates may be purely epitaxial due to the absence of subsurface rare earth atoms from previous preparations and a too low temperature to allow sufficient Tb diffusion into the substrate [Fig. 4(a) to (c)]. Not only for Dy silicide nanowires on Si(110), but also for Tb silicide nanowires on Si(001), it has been demonstrated that cross-sectional transmission electron microscopy data are very fruitful for structural characterization [10, 13]. Thus, we expect that such additional data for the various growth regimes will allow a conclusive structure determination in the future.

Before moving on to the discussion of the electronic properties of the Tb induced nanostructures, it has to be mentioned that the use of substrates not showing the 16 × 2 reconstruction, but ×5 structures probably induced by a slight Ni contamination, did not change the growth behavior found here. While an influence is certainly expected for low Tb coverage, the minimum coverage of 0.1 ML used here is presumably already too large to observe a contamination-induced effect. It is noted that Ni amounts as low as 0.007 ML may already lead to the transformation of the entire substrate [19].

3.2. Evolution of the electronic structure

3.2.1. The Si 2p core levels

The samples whose LEED patterns are depicted in Fig. 1 were also analyzed by PES. Fig. 6 shows some of the obtained Si 2*p* core-level spectra, which were normalized to have the same maximum height. In general, the width of the Si 2*p* spectra decreases when moving from 145 eV photon energy to 400 eV since the reduction of surface sensitivity leads to a stronger contribution from a sharp bulk component.

The measured spectra for the clean substrate agree very well with literature data [28]. For the Tb induced structures, the Si 2*p* spectra broaden and their spectral weights shift to lower binding energies. Furthermore, there is an apparent evolution of the spectra from wetting layer to nanowire dominated samples. At a binding energy of $E_{bin} \approx 98.7$ eV, a distinct shoulder is observed for the mixture of nanowires and wetting layer on the surface, which evolves into a clear peak for the nanowire dominated sample. In addition, the nanowire sample shows a small additional peak in surface sensitive measurements at $E_{bin} \approx 98.0$ eV. In contrast, the relative intensity at higher binding energies decreases with increasing nanowire concentration on the surface.

In order to obtain more detailed information, the spectra were analyzed by least-squares fits using spin–orbit split Pseudo-Voigt profiles [29]. To reduce the number of fit parameters, we assumed a fixed spin–orbit splitting of 0.60 eV with a fixed intensity ratio of 2 : 1

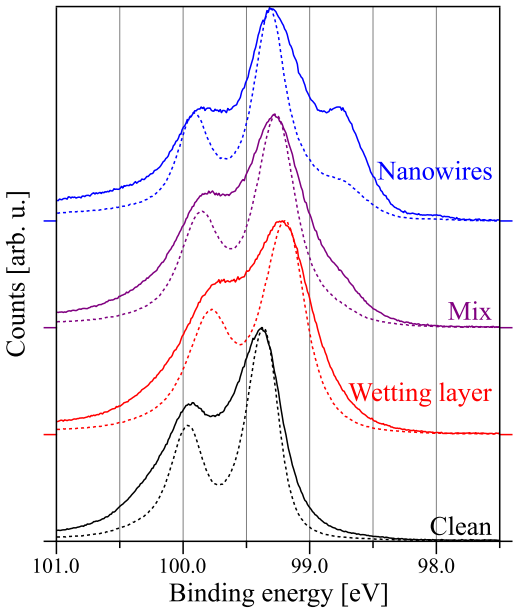

Fig. 6. Si 2*p* core-level spectra of Si(110) samples with varying Tb coverage, for which LEED patterns are depicted in Fig. 1. Continuous lines correspond to surface sensitive data obtained using a photon energy of $h\nu = 145$ eV, while dashed lines represent more bulk sensitive data ($h\nu = 400$ eV).

and included only a constant and a Shirley-type background. For each preparation, symmetric Pseudo-Voigt profiles with the same Gauss–Lorentz ratio [29] for all components was imposed. Example fit results for the various preparations are shown in Fig. 7(a) to (c).

Starting at low Tb coverage, the wetting layer spectra can be approximated using three main components, two broader ones and a narrower one in between them [Fig. 7(a)]. Based on the change of the relative areas of these components with surface sensitivity [Fig. 7(d)], the narrow component (blue) can be assigned to the Si bulk and the broader ones (bright and dark green) to the surface, i.e., the wetting layer. The core-level shifts of the wetting layer components with respect to the bulk component are $\Delta E_{CL} = -0.10$ eV for the one at lower binding energy and $\Delta E_{CL} = 0.23$ eV for the one at higher binding energy. In addition, there is a small and very broad component at high binding energy ($\Delta E_{CL} = 1.12$ eV). Such a component is often needed to fit Si 2*p* spectra and may be related to defects, to asymmetric line shapes, or to inelastic losses, e.g., caused by the adsorbate layers [30–33].

The Si 2*p* spectra of the sample with a mixture of wetting layer and nanowires can be described using the spectral composition obtained for the wetting layer spectra plus one additional component at lower binding energy (red), if one allows for small reductions of the line widths of the components [Fig. 7(b)]. Based on the dependence of the signal of the additional component on the photon energy [Fig. 7(d)], it is related to a surface structure. Thus, it is assigned to the nanowires. The observed core-level shift of this component with respect to the bulk component ($\Delta E_{CL} = -0.53$ eV) is very similar to the one observed for Tb disilicide nanostructures on planar and vicinal Si(111) ($\Delta E_{CL} = -0.52$ eV) [2,4], supporting the assumed formation of Tb disilicide nanowires.

Moving to the nanowire dominated sample, the Si 2*p* spectra are in principle well described by the same spectral composition as found for the mixture of wetting layer and nanowires [Fig. 7(c)]. However, a very weak component had to be included at $E_{bin} \approx 98.0$ eV (yellow). Furthermore, small reductions of the line widths are obtained in the fits, and the bulk component is observed to shift with respect to the other components by 0.07 eV to higher binding energy.

Based on these compositions of the Si 2*p* spectra, a consistent image emerges. While the wetting layer shows sharp spots in LEED patterns

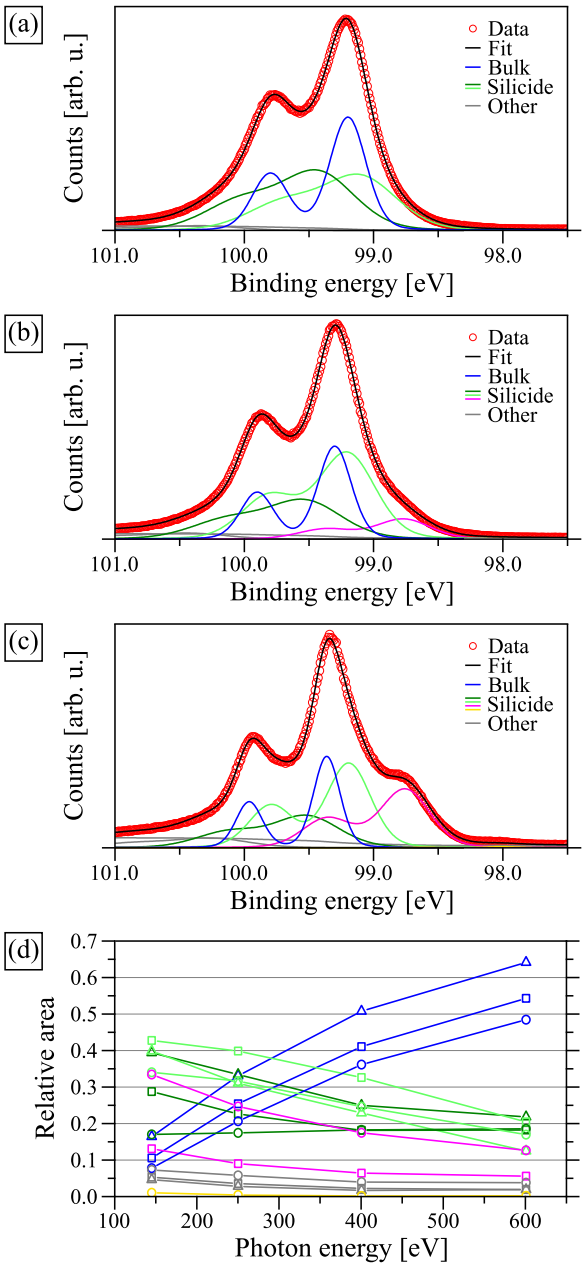

Fig. 7. Si 2*p* core-level spectra of (a) a pure wetting layer, (b) a mixture of wetting layer and nanowires, and (c) a nanowire dominated preparation and their deconvolutions into individual components ($h\nu = 250$ eV). (c) Dependence of the relative areas of the Si 2*p* core-level spectra components on the photon energy, i.e., the surface sensitivity. The same color scheme for the components as in (a) to (c) is used. Triangles mark the data for the wetting layer, squares those for the mixture of wetting layer and nanowires, and circles those for the nanowire dominated sample. The lines are guides for the eyes.

indicating global ordering, it is locally inhomogeneous, as observed by STM. This inhomogeneity leads to a manifold of similar, but in detail slightly varying Si atomic sites, e.g., by small variations in bond lengths or in chemical environment. Consequently, broad silicide components are found for the Si 2*p* spectra of the wetting layer [Fig. 7(a)].

Both the wetting layer and the nanowires consist of Tb and Si atoms. Thus, it may be assumed that they share analogous atomic configurations leading to Si atomic sites with similar core-level shifts. This assumption is supported by the observation of such a correlation between the Si 2*p* spectra of the wetting layer and the Tb silicide nanowires on Si(001) [33]. In the present case of the Si(110) substrate,

the nanowires are presumably characterized by a well-defined Tb silicide bulk structure. Thus, the rather similar Si atomic sites in the nanowires show less local variations than the ones of the inhomogeneous wetting layer. In conclusion, the nanowire formation does not only lead to new components in Si 2*p* spectra [magenta and yellow curves in Fig. 7(b) and (c)], but also to a narrowing of the components shared by the nanowires and the wetting layer [light and dark green curves in Fig. 7(b) and (c)].

Similarly, the line width of the Si bulk component reduces with increasing nanowire density, since the inhomogeneity of the surface band bending is reduced. As will be shown further below, the nanowires are metallic, while the wetting layer is semiconducting. For high nanowire coverage, the band bending induced by the nanowires thus dominates, furthermore leading to the observed small shift of the bulk component.

Moreover, the signal of the components solely related to the nanowires increases monotonously with nanowire density [magenta and yellow data in Fig. 7(d)]. In contrast, the intensity of the Si bulk component decreases monotonously with nanowire density [blue data in Fig. 7(d)], since the presumably endotaxially growing nanowires have a much larger thickness than the wetting layer with its extremely low Tb content, which thus encompasses only the topmost surface layers. As noted above, the silicide components assigned to the wetting layer are presumably shared with similar ones of the nanowires, resulting in rather complex intensity variations with nanowire density. However, when comparing the two components with each other, the wetting layer component at higher binding energy [dark green data in Fig. 7(d)] shows a smaller intensity decrease with decreasing surface sensitivity than the one at lower binding energy [light green data in Fig. 7(d)]. This trend is also observed for the other preparations, with the signal of the higher binding energy component even increasing with decreasing surface sensitivity for the nanowire dominated preparation, indicating that this component stems from deeper regions.

3.2.2. The Tb core levels and the valence bands

The continuous evolution from spectra dominated by the wetting layer to those dominated by nanowires is not only found in Si 2*p* core-level spectra, but also in the valence band spectra, which include the Tb 4*f* core level, and in Tb 5*p* core-level spectra [Fig. 8(a)]. As expected, the intensity of the Tb lines increases with increasing Tb coverage, but new features also arise in addition, e.g., a low binding energy shoulder in the Tb 5*p* core-level spectra and a high binding energy peak in the Tb 4*f* core-level spectra. Furthermore, taking a closer look at the Fermi level [Fig. 8(b)], the intensity is vanishing there for the wetting layer, but increases with increasing nanowire concentration, indicating a band gap for the wetting layer, while the nanowires are metallic.

The observation of a semiconducting wetting layer and metallic nanowires is in agreement with STS measurements (Fig. 9). The $I-V$-diagrams of the wetting layer always show a wide voltage range without tunneling current distinctly above the noise level ($\approx$ 0.5 pA) even when the tip is approached towards the sample [Fig. 9(a)]. Such a behavior is expected for an electronic structure with a band gap at the Fermi level. In STS spectra measured above a nanowire, in contrast, the narrow voltage region without measurable tunneling current vanishes monotonously with decreasing tip-sample distance, indicating a finite density of states at the Fermi level [Fig. 9(b)].

Thus, PES and STS data demonstrate that the nanowires represent a metallic surface structure, which is embedded in a semiconducting surrounding by the wetting layer and the Si substrate. Whether these anisotropic nanowires even show one-dimensional metallicity is studied in the following.

3.2.3. The electronic band structures

To elucidate the electronic dimensionality of the Tb induced nanostructures, ARPES measurements were performed. Fig. 10 shows overview band dispersion plots along the $\overline{\Gamma}-\overline{Y}$ and $\overline{\Gamma}-\overline{X}$ directions for the clean Si(110) substrate and samples with the various Tb induced

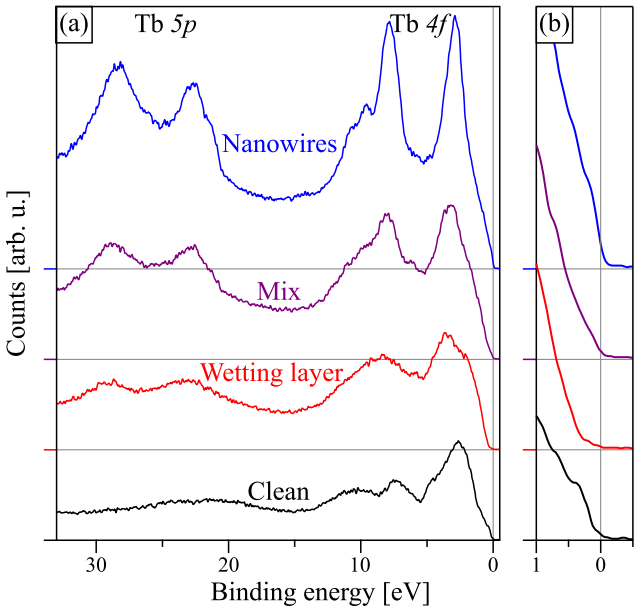

Fig. 8. (a) Valence band and Tb core-level spectra of surface preparations with increasing Tb coverage from bottom to top ($h\nu$ = 145 eV), and (b) detailed spectral region around the Fermi level. Corresponding LEED images of these samples are shown in Fig. 1.

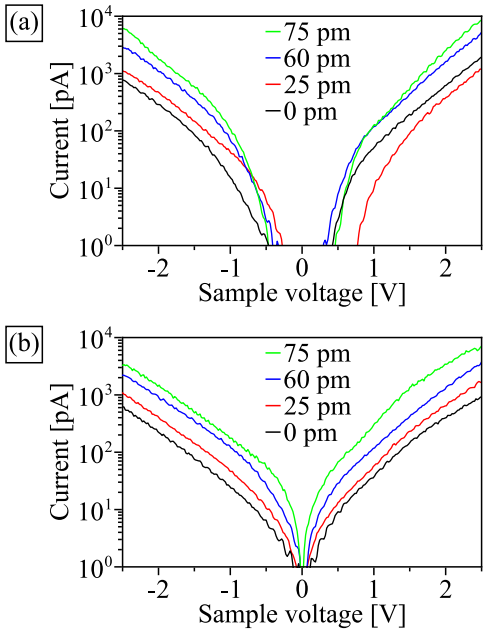

Fig. 9. Point STS spectra taken with the tip situated above (a) the wetting layer and (b) a nanowire. All measurements were performed with the same tip using the same stabilization conditions (V_S = −1.5 V and I_T = 100 pA) before turning off the feedback loop and approaching the sample by the tip displacements given in the diagrams.

nanostructures. The critical points $\overline{Y}$ and $\overline{X}$ are situated on the Brillouin zone boundary 5.8 nm^{-1} and 8.2 nm^{-1} away from $\overline{\Gamma}$ in the [001] and [1$\overline{1}$0] directions, respectively.

Starting with the clean Si(110) substrate [Fig. 10(a)], the dispersion plot is dominated by Si bulk bands. In addition, faint non-dispersive features are found at binding energies of $E_{bin} \approx 0.3$ eV and $E_{bin} \approx 0.8$ eV. The band near the Fermi level agrees well with the *S*1 and/or *S*2 surface state(s) discussed in the literature, while the energetic position

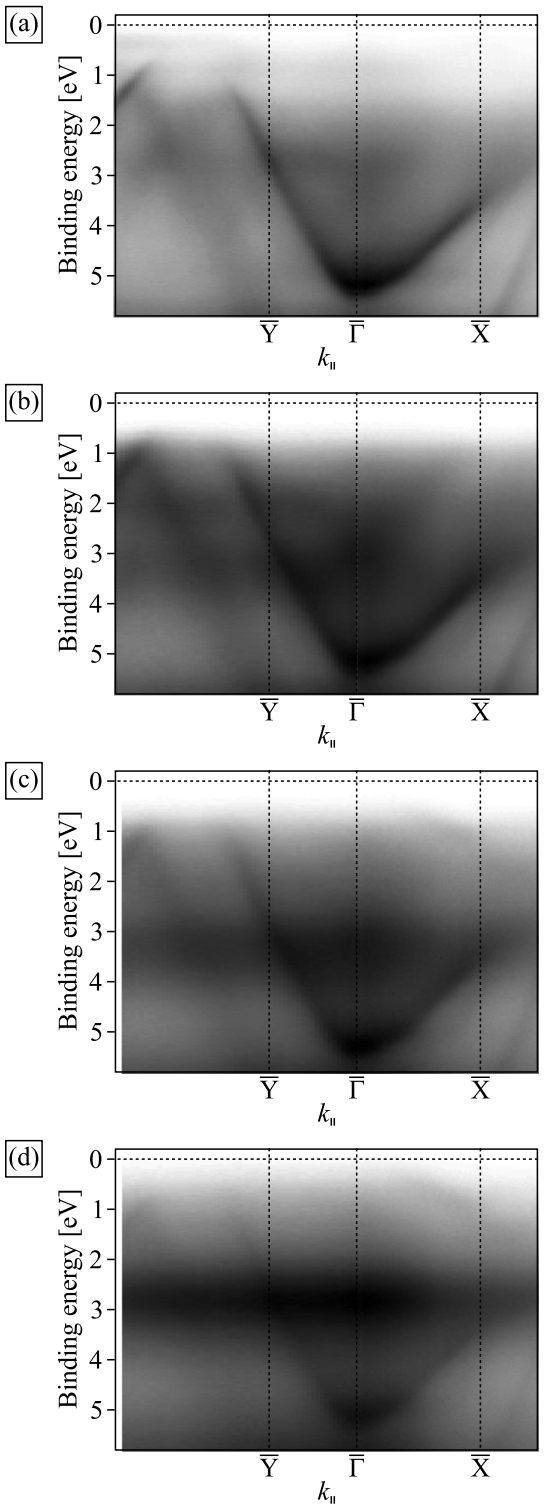

Fig. 10. Angle-resolved valence band overview data ($h\nu$ = 102 eV) for (a) a clean Si(110) substrate, (b) a wetting layer dominated sample, (c) a sample showing a mixture of nanowires and wetting layer, and (d) a nanowire dominated sample. Non-linear gray scales were used to highlight faint bands. The dashed horizontal lines mark the approximate Fermi level positions on which the binding energy scales are based.

of the lower band fits the $S3$ state [34]. This observation of the surface states again shows the good quality of the clean Si(110) substrates.

These surface states completely vanish upon formation of the Tb induced wetting layer [Fig. 10(b)], which is in agreement with the LEED and STM results showing a transformation of the entire substrate surface already for low Tb coverage [Figs. 1(b) and 2(b)]. This destruction of the surface states of the pristine substrate results in a considerable energy region near the Fermi level without substantial intensity supporting the above findings of a wetting layer with a band gap. Furthermore, the Si bulk bands appear less sharp for the wetting layer dominated sample and additional non-dispersive features are observed for $E_{\mathrm{bin}} \approx 2.0$ eV and between $E_{\mathrm{bin}} \approx 3.0$ eV and $E_{\mathrm{bin}} \approx 4.0$ eV.

The latter feature is related to the Tb $4f$ core level and its relative intensity increases with Tb coverage [Fig. 10(c) and (d)]. However, the feature around $E_{\mathrm{bin}} \approx 2.0$ eV is not distinguishable anymore for samples showing a mixture of wetting layer and nanowires [Fig. 10(c)]. Thus it may be related solely to the wetting layer, possibly to a chemically shifted Tb $4f$ component, as also indicated by the shoulder at $E_{\mathrm{bin}} \approx 2.0$ eV in Fig. 8(a).

Upon nanowire formation, a new strongly dispersing band is observed near the Fermi level around the $\overline{\mathrm{X}}$ point [Fig. 10(c) and (d)]. This band is only barely visible in Fig. 10 because of the dominating features at higher binding energies, but it is more intense for increased nanowire density, signifying that it stems from the Tb silicide nanowires. Furthermore, it is the only clear feature observed within the apparent band gap of the substrate, i.e., for $E_{\mathrm{bin}} < 0.8$ eV.

In order to analyze this nanowire related band further, a more detailed view on the band structure close to the Fermi level is given in Fig. 11. In the dispersion plot through the Brillouin zone center in $[1\bar{1}0]$ direction, i.e., along the nanowires, the band is easily discernible [Fig. 11(a)]. Unfortunately, the expected Fermi level crossing of this band is not visible, presumably due to photoemission matrix element effects, but can be extrapolated to $|k_{[1\bar{1}0]}| \approx 1.5$ nm^{-1} assuming a continuing almost linear dispersion up to the Fermi level. In contrast, the bottom of this band is directly determinable, especially, when using dispersion plots in which the band is also distinguishable for $|k_{[1\bar{1}0]}| > 8.2$ nm^{-1} [Fig. 11(b)]. It lies at the Brillouin zone boundary $k_{[1\bar{1}0]} = 8.2$ nm^{-1} and about 1.0 eV below the Fermi level. The approximate band dispersion is indicated in Fig. 11(a) and (b) by dashed lines.

At the bottom of this band, an almost parabolic dispersion is observed, corresponding to an effective mass of $m^* \approx 0.7\ m_0$ (evaluation range $\Delta k_{[1\bar{1}0]} = \pm 2$ nm^{-1}), where m_0 is the free-electron mass. This value is comparable to those obtained for Tb silicide nanowires on Si(001) ranging from $\approx 0.2\ m_0$ to $\approx 1.1\ m_0$ [33], as well as to those obtained for two-dimensional Tb silicide monolayer films on Si(111), being strongly anisotropic with components of $\approx 0.16\ m_0$ and $\approx 1.45\ m_0$ [2].

Dispersion plots through this band in [001] direction show no dispersion, indicating a quasi-one-dimensional characteristic, as expected for these rather thin metallic nanowires in a semiconducting environment. However, an even more compelling proof for the quasi-one-dimensional nature of this band is obtained from inspecting constant binding energy surfaces. There, purely one-dimensional bands are characterized by linear contours, while two- or three-dimensional signatures typically form closed lines such as ellipses. On the energy surface near the band bottom depicted in Fig. 11(c), the linear energy contours of the band are clearly seen, as indicated by the arrows. This impression is solidified for further energy contour plots, e.g., the one at $E_{\mathrm{bin}} \approx 0.3$ eV [Fig. 11(d)], where the straight contours of the band are well resolved within the first Brillouin zone. Thus the nanowires are characterized by a quasi-one-dimensional band, which presumably crosses the Fermi level. The latter assumption is supported by the finite density of states observed in valence-band PES [Fig. 8(b)] and the behavior of the STS spectra [Fig. 9(b)]. It has to be noted that the strong intensity on the energy surfaces around $k_{[1\bar{1}0]} = 0$ for $k_{[001]} > 5.8$ nm^{-1} was observed for all samples. Thus, it cannot be related to the nanowires.

The observation of only one single band clearly assigned to the Tb silicide nanowires may appear surprising, since more bands are expected, also at higher binding energies. However, an ensemble of

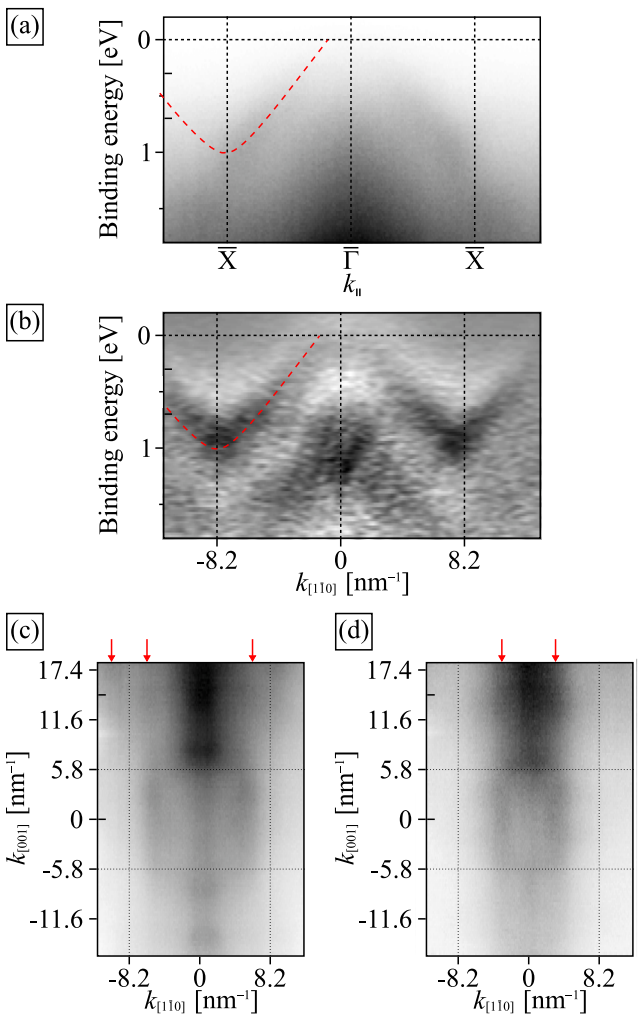

Fig. 11. Detailed ARPES data for the nanowire dominated sample. (a, b) Dispersion plots near the Fermi level for (a) $k_{[001]} = 0$ and (b) $k_{[001]} = 14.5$ nm^{-1}. The second derivative is shown in (b) to highlight the faint quasi-one-dimensional band. The red dashed lines mark the approximate dispersion of this band. (c, d) Constant energy surfaces for (c) $E_{bin} \approx 0.7$ eV and (d) $E_{bin} \approx 0.3$ eV, with the arrows marking the quasi-one-dimensional band. The inner ticks in (a) and (b) mark the positions where the plots (c) and (d) were extracted from the three-dimensional data set and *vice versa*.

nanowires with varying sizes is probed by ARPES leading to a superposition of the signals from the individual band structures. Consequently, the quasi-one-dimensional band observed here presumably stems from a structure common to many nanowires and may be related to a distinct surface, edge, or interface state. A similar observation of an edge state was made for Tb silicide nanowires on vicinal Si(111) substrates [5].

4. Conclusion

In this work, we studied the growth of Tb induced structures on Si(110) and characterized them by LEED, STM, STS, core-level and valence band PES, and ARPES. Initially, a wetting layer forms for low Tb coverage and, with increasing Tb coverage, the surface is continuously covered by unidirectional Tb silicide nanowires as observed in STM and confirmed by LEED and (AR)PES. Thereby, extremely high aspect ratios of the nanowires are obtained for high annealing temperatures or samples already containing Tb in the bulk. Both wetting layer and nanowires are stable for temperatures up to 750 °C at least for a short annealing period.

The nanowires are characterized by a finite density of states at the Fermi level, while the wetting layer shows a band gap. Thus, the metallic nanowires are embedded in a semiconducting surrounding. In addition, a quasi-one-dimensional band was observed for the nanowires in ARPES. Thus, this system is an interesting candidate to search for unique one-dimensional properties of the nanowires, such as a Peierls transition at low temperatures [6]. Furthermore, these nanowires are prime candidates to study the influence of electronic interactions between neighboring nanowires, since their density and therewith their separation can be tuned by the Tb coverage and since no long-range interactions via the substrate or the wetting layer are expected due to their semiconducting nature.

CRediT authorship contribution statement

Stephan Appelfeller: Conceptualization, Investigation, Software, Validation, Formal analysis, Visualization, Writing – original draft, Supervision, Project administration, Data curation. **Martin Franz:** Investigation, Writing – review & editing. **Murat Karadag:** Investigation, Formal analysis. **Milan Kubicki:** Investigation. **Robert Zielinski:** Investigation. **Maxim Krivenkov:** Investigation, Resources, Software, Writing – review & editing. **Andrei Varykhalov:** Investigation, Resources, Writing – review & editing. **Alexei Preobrajenski:** Investigation, Resources, Writing – review & editing. **Mario Dähne:** Conceptualization, Validation, Supervision, Project administration, Writing – review & editing, funding acquisition.

Declaration of competing interest

The authors declare that they have no known competing financial interests or personal relationships that could have appeared to influence the work reported in this paper.

Data availability

Data will be made available on reasonable request.

Acknowledgments

This work was supported by the Deutsche Forschungsgemeinschaft, Germany through FOR 1700 project E2 (project no. DA 408/19-2). We acknowledge MAX IV Laboratory for time on FlexPES and in the STM-Laboratory under proposals 20200270 and 20200663, respectively. Research conducted at MAX IV, a Swedish national user facility, is supported by the Swedish Research council, Sweden under contract 2018-07152, the Swedish Governmental Agency for Innovation Systems, Sweden under contract 2018-04969, and Forma, Sweden under contract 2019-02496. ARPES measurements were carried out at the 1^2 ARPES station at the BESSY II electron storage ring operated by the Helmholtz-Zentrum Berlin für Materialien und Energie [35]. The XPST program package by M. Schmid for Igor Pro was used for the analysis of core-level PES data.

References

[1] M.V. Bulanova, A.N. Mikolenko, K.A. Meleshevich, G. Effenberg, P.A. Saltykov, Terbium-silicon system, Z. Met.kd. 90 (1999) 216.
[2] M. Franz, S. Appelfeller, C. Prohl, J. Große, H.-F. Jirschik, V. Füllert, C. Hassenstein, Z. Diemer, M. Dähne, Growth and electronic properties of Tb silicide layers on Si(111), J. Vac. Sci. Technol. A 34 (2016) 061503, http://dx.doi.org/10.1116/1.4964132.
[3] S. Appelfeller, S. Kuls, M. Dähne, Tb silicide nanowire growth on planar and vicinal Si(001) surfaces, Surf. Sci. 641 (2015) 180, http://dx.doi.org/10.1016/j.susc.2015.07.001.
[4] S. Appelfeller, M. Franz, L. Freter, C. Hassenstein, H.-F. Jirschik, M. Dähne, Growth and characterization of tb silicide nanostructures on Si(*hhk*) substrates, Phys. Rev. Mater. 3 (2019) 126002, http://dx.doi.org/10.1103/PhysRevMaterials.3.126002.
[5] S. Appelfeller, K. Holtgrewe, M. Franz, L. Freter, C. Hassenstein, H.-F. Jirschik, S. Sanna, M. Dähne, Continuous crossover from two-dimensional to one-dimensional electronic properties for metallic silicide nanowires, Phys. Rev. B 102 (2020) 115433, http://dx.doi.org/10.1103/physrevb.102.115433.

[6] R.E. Peierls, Quantum Theory of Solids, Oxford University Press, Oxford New York, [1955], 2001, http://dx.doi.org/10.1093/acprof:oso/9780198507819.001.0001.

[7] K.S. Novoselov, A.K. Geim, S.V. Morozov, D. Jiang, M.I. Katsnelson, I.V. Grigorieva, S.V. Dubonos, A.A. Firsov, Two-dimensional gas of massless Dirac fermions in graphene, Nature 438 (2005) 197, http://dx.doi.org/10.1038/nature04233.

[8] C.H. Luo, F.R. Chen, L.J. Chen, Atomic structure of Si/$TbSi_2$/(111)Si double-heterostructure interfaces, J. Appl. Phys. 76 (1994) 5744, http://dx.doi.org/10.1063/1.358411.

[9] S. Appelfeller, M. Franz, M. Kubicki, R. Paul, T. Niermann, M.A. Schubert, M. Lehmann, M. Dähne, Capping of rare earth silicide nanowires on Si(001), Appl. Phys. Lett. 108 (2016) 013109, http://dx.doi.org/10.1063/1.4939693.

[10] S. Appelfeller, J. Heggemann, T. Niermann, M. Lehmann, M. Dähne, Refined structure model of rare earth silicide nanowires on Si(001), Appl. Phys. Lett. 114 (2019) 093104, http://dx.doi.org/10.1063/1.5086369.

[11] M. Franz, J. Große, R. Kohlhaas, M. Dähne, Terbium induced nanostructures on Si(111), Surf. Sci. 637–638 (2015) 149, http://dx.doi.org/10.1016/j.susc.2015.03.026.

[12] S. Sanna, C. Dues, W.G. Schmidt, F. Timmer, J. Wollschläger, M. Franz, S. Appelfeller, M. Dähne, Rare-earth silicide thin films on the Si(111) surface, Phys. Rev. B 93 (2016) 195407, http://dx.doi.org/10.1103/PhysRevB.93.195407.

[13] Z. He, M. Stevens, D.J. Smith, P.A. Bennett, Dysprosium silicide nanowires on Si(110), Appl. Phys. Lett. 83 (2003) 5292, http://dx.doi.org/10.1063/1.1636244.

[14] I.-H. Hong, Y.-F. Tsai, T.-M. Chen, Self-organization of mesoscopically ordered parallel Gd-silicide nanowire arrays on a Si(110)-16 × 2 surface: A massively parallel active architecture, Appl. Phys. Lett. 98 (2011) 193118, http://dx.doi.org/10.1063/1.3590199.

[15] S.M. Hus, H.H. Weitering, Formation of uni-directional ultrathin metallic YSi_2 nanowires on Si(110), Appl. Phys. Lett. 103 (2013) 073101, http://dx.doi.org/10.1063/1.4817529.

[16] I. Horcas, R. Ferná, J.M. Gómez-Rodríguez, J. Colchero, J. Gómez-Herrero, A.M. Baro, WSXM: A software for scanning probe microscopy and a tool for nanotechnology, Rev. Sci. Instrum. 78 (2007) 013705, http://dx.doi.org/10.1063/1.2432410.

[17] D. Nečas, P. Klapetek, Gwyddion: an open-source software for SPM data analysis, Open Phys. 10 (2012) 181, http://dx.doi.org/10.2478/s11534-011-0096-2.

[18] H. Ampo, S. Miura, K. Kato, Y. Ohkawa, A. Tamura, Atomic configuration of hydrogenated and clean Si(110) surfaces, Phys. Rev. B 34 (1986) 2329, http://dx.doi.org/10.1103/physrevb.34.2329.

[19] E.J. Loenen, D. Dijkkamp, A.J. Hoeven, Clean and metal-contaminated si(110) surfaces studied by RHEED, XPS and STM, J. Microsc. 152 (1988) 487, http://dx.doi.org/10.1111/j.1365-2818.1988.tb01412.x.

[20] Y. Yamada, A. Girard, H. Asaoka, H. Yamamoto, S. i. Shamoto, Single-domain Si(110) – 16 × 2 surface fabricated by electromigration, Phys. Rev. B 76 (2007) 153309, http://dx.doi.org/10.1103/PhysRevB.76.153309.

[21] N.K. Lewis, N.B. Clayburn, E. Brunkow, T.J. Gay, Y. Lassailly, J. Fujii, I. Vobornik, W.R. Flavell, E.A. Seddon, Domain formation mechanism of the Si(110) 16 × 2 reconstruction, Phys. Rev. B 95 (2017) 205306, http://dx.doi.org/10.1103/physrevb.95.205306.

[22] W.E. Packard, J.D. Dow, Si(110)-16 × 2 and Si(110)-5 × 1 surface reconstructions: Stretched-hexagon face-centered adatom model, Phys. Rev. B 55 (1997) 15643, http://dx.doi.org/10.1103/PhysRevB.55.15643.

[23] T. Ichinokawa, H. Ampo, S. Miura, A. Tamura, Formation of surface superstructures by heat treatments on Ni-contaminated surface of Si(110), Phys. Rev. B 31 (1985) 5183, http://dx.doi.org/10.1103/PhysRevB.31.5183.

[24] S. Chandola, E. Speiser, N. Esser, S. Appelfeller, M. Franz, M. Dähne, Optical anisotropy of quasi-1D rare-earth silicide nanostructures on Si(001), Appl. Surf. Sci. 399 (2017) 648, http://dx.doi.org/10.1016/j.apsusc.2016.12.044.

[25] I.-H. Hong, Y.-C. Liao, Y.-F. Tsai, Template-directed atomically precise self-organization of perfectly ordered parallel cerium silicide nanowire arrays on Si(110)-16 × 2 surfaces, Nanoscale Res. Lett. 8 (2013) 458, http://dx.doi.org/10.1186/1556-276x-8-458.

[26] I.-H. Hong, Self-organization of mesoscopically-ordered parallel rare-eath silicide nanowire arrays on Si(110)-16 × 2 surface, in: Nanofabrication, InTech, 2011, http://dx.doi.org/10.5772/27403.

[27] J. Tersoff, R.M. Tromp, Shape transition in growth of strained islands: Spontaneous formation of quantum wires, Phys. Rev. Lett. 70 (18) (1993) 2782–2785, http://dx.doi.org/10.1103/physrevlett.70.2782.

[28] N.D. Kim, Y.K. Kim, C.-Y. Park, H.W. Yeom, H. Koh, E. Rotenberg, J.R. Ahn, High-resolution photoemission spectroscopy study of the single-domain Si(110)-16 × 2 surface, Phys. Rev. B 75 (2007) 125309, http://dx.doi.org/10.1103/physrevb.75.125309.

[29] M. Schmid, H.-P. Steinrück, J.M. Gottfried, A new asymmetric Pseudo-Voigt function for more efficient fitting of XPS lines, Surf. Interface Anal. 46 (2014) 505, http://dx.doi.org/10.1002/sia.5521.

[30] C.J. Karlsson, E. Landemark, Y.-C. Chao, R.I.G. Uhrberg, Atomic origins of the surface components in the Si 2p core-level spectra of the Si(111)7×7 surface, Phys. Rev. B 50 (1994) 5767, http://dx.doi.org/10.1103/PhysRevB.50.5767.

[31] T.-W. Pi, I.-H. Hong, C.-P. Cheng, G.K. Wertheim, Surface photoemission from Si(100) and inelastic electron mean-free-path in silicon, J. Electron. Spectrosc. 107 (2000) 163, http://dx.doi.org/10.1016/S0368-2048(00)00099-2.

[32] P.E.J. Eriksson, R.I.G. Uhrberg, Surface core-level shifts on clean Si(001) and Ge(001) studied with photoelectron spectroscopy and density functional theory calculations, Phys. Rev. B 81 (2010) 125443, http://dx.doi.org/10.1103/PhysRevB.81.125443.

[33] S. Appelfeller, M. Franz, H.-F. Jirschik, J. Große, M. Dähne, The electronic structure of Tb silicide nanowires on Si(001), New J. Phys. 18 (2016) 113005, http://dx.doi.org/10.1088/1367-2630/18/11/113005.

[34] K. Sakamoto, M. Setvin, K. Mawatari, P.E.J. Eriksson, K. Miki, R.I.G. Uhrberg, Electronic structure of the Si(110) – (16 × 2) surface: High-resolution ARPES and STM investigation, Phys. Rev. B 79 (2009) 045304, http://dx.doi.org/10.1103/PhysRevB.79.045304.

[35] A. Varykhalov, Helmholtz-Zentrum Berlin für materialien und energie, 1^2-ARPES: The ultra high resolution photoemission station at the U112-PGM-2a-1^2 beamline at BESSY II, J. Large-Scale Res. Fac. 4 (2018) A128, http://dx.doi.org/10.17815/jlsrf-4-99.